# Kondo behavior, ferromagnetic correlations, and crystal fields in the heavy Fermion compounds $Ce_3X$ ( X=In, Sn)

C. H. Wang[1,2], J. M. Lawrence[1], A. D. Christianson[3], E. A. Goremychkin[4], V. R. Fanelli[2], K. Gofryk[2], E. D. Bauer[2], F. Ronning[2], J. D. Thompson[2], N. R. de Souza[4,5], A. I. Kolesnikov[3], K. C. Littrell[3]

[1] *University of California, Irvine, California 92697, USA*

[2] *Los Alamos National Laboratory, Los Alamos, NM 87545, USA*

[3] *Neutron Scattering Sciences Division, Oak Ridge National Laboratory, Oak Ridge, TN, 37831, USA*

[4] *Argonne National Laboratory, Argonne, IL 60439, USA*

[5] *Australian Nuclear Science and Technology Organisation, Lucas Heights, NSW 2234, Australia*

(Dated: March 19, 2010)

We report measurements of inelastic neutron scattering, magnetic susceptibility, magnetization, and the magnetic field dependence of the specific heat for the heavy Fermion compounds $Ce_3In$ and $Ce_3Sn$. The neutron scattering results show that the excited crystal field levels have energies $E_1$ = 13.2 meV, $E_2$ = 44.8 meV for $Ce_3In$ and $E_1$ = 18.5 meV, $E_2$ = 36.1 meV for $Ce_3Sn$. The Kondo temperature deduced from the quasielastic linewidth is 17 K for $Ce_3In$ and 40 K for $Ce_3Sn$. The low temperature behavior of the specific heat, magnetization, and susceptibility can not be well-described by J=1/2 Kondo physics alone, but require calculations that include contributions from the Kondo effect, broadened crystal fields, and ferromagnetic correlations, all of which are known to be important in these compounds. We find that in $Ce_3In$ the ferromagnetic fluctuation makes a 10-15 % contribution to the ground state doublet entropy and magnetization. The large specific heat coefficient $\gamma$ in this heavy fermion system thus arises more from the ferromagnetic correlations than from the Kondo behavior.



## I. INTRODUCTION

In heavy fermion (HF) compounds, it is very common to establish the Kondo energy scale $T_K$ from the linear coefficient of specific heat $\gamma$ through Rajan's formula $T_K = \pi JR/3\gamma_0$ derived for the degenerate $(2J+1 \geq 2)$ Kondo model[1] where $J$ is the total angular momentum. In previous studies of the specific heat of the HF compounds $Ce_3X$ (X=In, Sn)[2,3] which crystallize in the $Cu_3Au$ cubic structure, this formula was used to determine the Kondo temperature, which was found to be 4.8 K for $Ce_3In$ and 16.7 K for $Ce_3Sn$. The crystal electric field (CEF) excitation energy was estimated to be $T_{CEF}$=65 K.

Most HF compounds reside close to a quantum critical point (QCP)where antiferromagnetic (AFM) or ferromagnetic (FM) correlations are present. This makes the previous analysis inappropriate in so far as it assumes that the magnetic correlations do not contribute to $\gamma$. Indeed, the Wilson ratios $(\pi^2 R\chi_0/3C_J\gamma_0)$ which were determined previously for $Ce_3In$ and $Ce_3Sn$ are 11.5 and 7.0 respectively[2,3], indicating that ferromagnetic correlations dominate the susceptibility.

Inelastic neutron scattering(INS) experiments on single crystals of compounds that are close to a QCP, such as $CeRu_2Si_2$[4] or $CeNi_2Ge_2$[5] exhibit two classes of excitations. At most $Q$ in the Brillouin zone, the scattering has the characteristic Kondo energy dependence and is $Q$-independent or only weakly $Q$-dependent. Similar behavior is observed in intermediate valence compounds for which it is clear that the behavior of the low temperature susceptibility, specific heat and INS spectra are close to the Kondo impurity prediction, as though the onset of lattice coherence has only a minor effect on these measurements[6,7]. Near the QCP, however, large $Q$-dependent scattering is observed with maximum intensity at the critical wavevector $Q_c$ ($Q_c$ = 0 for FM and $Q_c = Q_N$ for AFM) where ordering occurs in the nearby magnetic state. This scattering represents the short range order. It is dynamic and critically slows down, or softens, as the QCP is approached by lowering the temperature or changing a control parameter. These fluctuations affect the specific heat and can result in non-Fermi liquid behavior.

Hence INS in single crystals can separate the Kondo behavior from the contributions due to magnetic correlations. Since the spectral weight in the magnetic correlations is typically small, INS in polycrystals will be dominated by the $Q$-independent Kondo scattering. INS can also be used to directly determine the CEF excitations. Under these circumstance, INS provides a better way to determine $T_K$ and $E_{CEF}$ than through analysis of the specific heat. In this paper, we employ INS to determine both $T_K$ and $E_{CEF}$. We have re-measured the magnetic susceptibility, and have extended the specific heat measurement, which in the previous report was measured down to 1.8 K in zero applied magnetic field, to $T$ = 400 mK and $B$ = 9T. We have also measured the low temperature magnetization to 13 T.

In the $Ce_3X$ compounds, the Ce ions sit on the face centers of the cubic lattice and are subject to a crystalline electric field (CEF) of tetragonal symmetry. In this case, the Hamiltonian is described as:

$$H_{CF} = B_2^0 O_2^0 + B_4^0 O_4^0 + B_4^4 O_4^4,$$

where $B_l^m$ and $O_l^m$ are the crystal field parameters and Steven operators, respectively. The sixfold degenerate $4f^1$, J=5/2 state splits into three doublets.

Diagonalizing the Hamiltonian, the atomic wave functions are given by:[8,9]

$\Gamma_7^{(1)} = \eta|\pm 5/2> + \sqrt{1-\eta^2}|\mp 3/2>$
$\Gamma_7^{(2)} = \sqrt{1-\eta^2}|\pm 5/2> - \eta|\mp 3/2>$
$\Gamma_6 = |\pm 1/2>$

Depending on the admixture of the $J$=5/2 and 3/2 states, the inelastic neutron scattering spectra will exhibit one or two inelastic excitations. Low energy transfer quasielastic scattering will also be observed if the instrumental resolution is adequate. From the INS spectra, the crystal field energies and wavefunctions can be determined from the ampitudes and energies of the excitations. The Kondo effect, which arises from the hybridization of the 4 $f$-electron with the conduction electrons, broadens the peak line-widths proportional to $k_BT_K$. The quasielastic scattering peak width $\Gamma_{QE}$ can be equated to the Kondo energy $k_BT_K$ of the ground state doublet.

In what follows, we will use the CEF parameters and the Kondo energies derived from the neutron scattering to calculate the Kondo contribution to the specific heat, susceptibility and magnetization. All the Kondo calculations utilized[1,10,11] employ the same Bethe-Ansatz calculation, making intercomparison possible.

## II. EXPERIMENT

All samples were prepared by arc melting in an ultra-high-purity argon atmosphere. After melting the samples were sealed under vacuum and annealed at $500^0$C for 2 weeks and cooled slowly to room temperature. The magnetization was measured in a 14 T Quantum Design Vibrating Sample Magnetometer at the National High Magnetic Field Laboratory (NHMFL) at Los Alamos National Laboratory. The specific heat was measured in a Quantum Design PPMS system. The magnetic susceptibility measurements were performed in a commercial superconducting quantum interference device (SQUID) magnetometer.

We performed inelastic neutron scattering on a 29 gram sample of $Ce_3In$ and a 37 gram sample of $Ce_3Sn$ using the high energy transfer chopper spectrometer (HET) at ISIS (at the Rutherford Appleton Laboratory) and the low resolution medium energy chopper spectrometer (LRMECS) at IPNS (at Argonne National Laboratory). For $Ce_3Sn$, the quasi-elastic neutron spectrometer (QENS, at IPNS) was also used to measure the low energy scattering. To increase the dynamic range of the INS spectrum, a variety of incident energies ($E_i$ = 15 meV, 35 meV, 60 meV, 100 meV for HET and 35 meV for LRMECS) and temperatures ( 4.5 K, 100 K, 150 K, 200 K and 250 K for HET; 10K, 100K, 150K for LRMECS) were employed. The HET data have been normalized to vanadium to establish the absolute value. All the data have been corrected for absorption ( which is very obvious for $Ce_3In$ case), total scattering cross section, and sample mass.

For the HET data, the low Q data were obtained from averaging the low angle detectors with angles ranging from 11.5 degrees to 26.5 degrees. The high Q data were obtained from the high angle detector bank at an angle 136 degrees. For the LRMECS experiment, the low Q data were obtained by averaging over the low angle detectors with average angle equal to 13 degrees; and the high Q data were obtained from high angle detectors where the average angle was 87 degrees. The QENS data were collected at 7 K. This inverse geometry spectrometer has 19 detector banks with $Q$ from $Q = 0.36$ to $Q = 2.52$, each with a slightly different final energy ($E_f$ from 2.82 meV to 3.36 meV). For every fixed $Q$, we removed the Ce $4f$ form factor to obtain a spectrum representing the $Q = 0$ scattering and then summed all 19 spectra together to obtain a total $S(Q = 0, \Delta E)$ spectrum. In order to compare the QENS spectrum with the spectra from the direct geometry spectrometers HET and LRMECS, we multiplied the QENS spectrum $S(Q = 0, \Delta E)$ by the $4f$ form factor apppropriate for HET at $E_i$ = 35 meV.

To subtract the nonmagnetic (background, single phonon, and multiple phonon) contributions, we measured the non-magnetic counterpart compounds $La_3In$ and $La_3Sn$. For the specific heat, we obtained the magnetic contribution by direct subtraction, i.e. $C_{mag} = C(Ce) - C(La)$. For the INS data we used $La_3In$ and $La_3Sn$ to determine the scaling of the nonmagnetic scattering between low $Q$ and high $Q$ as $h(\Delta E) = S(La, LQ)/S(La, HQ)$. Using this factor we scaled the high $Q$ data (where the nonmagnetic scattering dominates) to the low $Q$ data (where the magnetic scattering dominates) in Ce compounds to determine the nonmagnetic contribution[12–14].

## III. RESULTS AND DISCUSSION

Fig. 1(a) and (c) directly compare the low $Q$ INS spectra of $Ce_3In$ and $La_3In$; the data were collected on HET with incident energy $E_i$ = 15 meV (a) and 60 meV (c) at 4.5 K. Fig. 1(b) compares the low $Q$ and high $Q$ data for $Ce_3In$ collected on LRMECS with an incident energy $E_i$= 35 meV at 10 K. The low $Q$ data for $Ce_3Sn$ and $La_3Sn$, which were collected on HET, are compared in Fig. (d), (e) and (f) where the incident energies are $E_i$=15 meV (d), 35 meV (e) and 60 meV (f) at 4.5 K. In these spectra, two excited energy levels, corresponding to crystal field excitations, are observed for both $Ce_3In$ and $Ce_3Sn$. The spectra (a) and (d), which compare the $Ce_3In$(Sn) and $La_3In$(Sn) scattering at low energy transfer ($\Delta E <$ 9 meV), exhibit obvious quasielastic scattering which as mentioned above arises from Kondo scattering.

The magnetic contribution $S_{mag}$ to the scattering of $Ce_3In$, obtained using the method described above, is shown in Fig. 2. The solid lines represent a fit to the CEF model. Since the inelastic peaks are

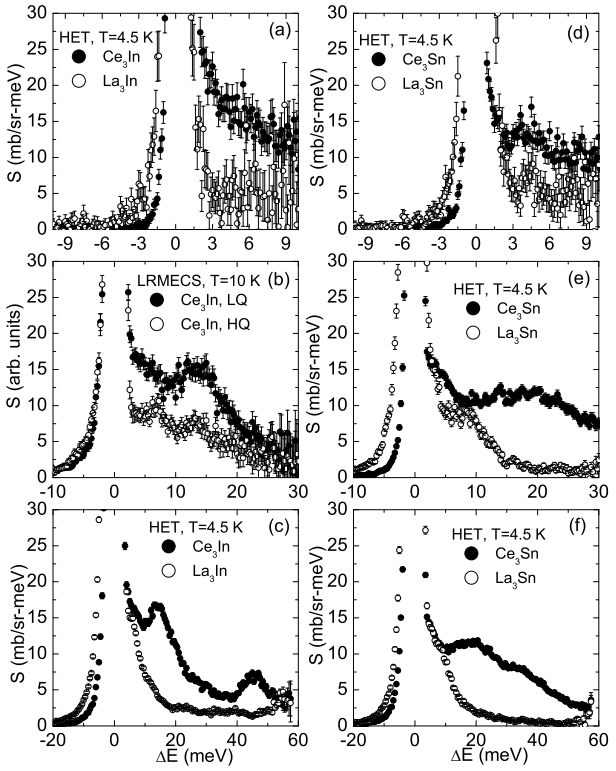


FIG. 1: Inelastic neutron scattering spectra for $Ce_3In$ and $Ce_3Sn$ together with that of their nonmagnetic counterpart compounds obtained from HET and LRMECS. The data collected on HET are at 4.5 K and on LRMECS are at 10 K. (a) $E_i$=15 meV, (b) $E_i$=35 meV, and (c) $E_i$=60 meV spectra of $Ce_3In$ and $La_3In$. (d) $E_i$=15 meV, (e) $E_i$=35 meV and (f) $E_i$=60 meV spectra for $Ce_3Sn$ and $La_3Sn$. All spectra are for low $Q$ except in (b) where a high-$Q$ spectrum is included for comparison.

relatively broad, the line widths $\Gamma_i$ are taken to be finite. In this case, the magnetic scattering is described as:

$$S_{mag} = \frac{2N}{\pi\mu_B^2} f^2(Q)(1 - e^{-\Delta E/k_B T})\chi''(Q, \Delta E)$$

$$\chi''(Q, \Delta E) = \Sigma\chi_i(T)\Delta E(\frac{\Gamma_i}{2\pi})/[(\Delta E - E_i)^2 + \Gamma_i^2]$$

Here $i$=0,1,2, $E_0 = 0$ corresponds to the quasielastic scattering, and $f^2(Q)$ is the Ce $4f$ form factor. The CEF model fitting was performed simultaneously on six data sets at three different incident energies ($E_i$=15 meV, 35 meV and 60 meV) and at two different temperatures (4.5 K and 150 K). Fig. 2(a)-(d) are the data collected on HET. In Fig. 2(f) the LRMECS data are displayed for comparison. The resulting CEF fitting parameters are shown in Table I. The ground state is the $\Gamma_7^{(1)}$ doublet, the first excited state is the $\Gamma_7^{(2)}$ doublet[15] at the energy 13.2 meV, and the second excited state is the $\Gamma_6$ doublet at the energy 44.8 meV. The quasielastic line width $\Gamma_{QE} = \Gamma_0 = 1.49$ meV, implies that $T_K = \Gamma_{QE}/k_B = 17$ K.

TABLE I: CEF model fitting parameters for $Ce_3In$ and $Ce_3Sn$.

| | $Ce_3In$ | $Ce_3Sn$ |
|---|---|---|
| $B_2^0$(meV) | -2.203±0.015 | -1.660±0.017 |
| $B_4^0$(meV) | 0.066±0.001 | 0.038±0.0009 |
| $B_4^4$(meV) | -0.154±0.004 | -0.263±0.003 |
| $\eta$ | 0.94 | 0.89 |
| $E_1$ (meV) | 13.2 | 18.5 |
| $E_2$ (meV) | 44.8 | 36.1 |
| $\Gamma_{QE}$ (meV) | 1.49±0.07 | 3.52±0.16 |
| $\Gamma_1$ (meV) | 5.98±0.07 | 9.37±0.038 |
| $\Gamma_2$ (meV) | 2.06±0.37 | 6.28±0.38 |
| $\chi^2$ | 2.4057 | 2.1528 |
| $\lambda$ (mole-Ce/emu) | 62 | 85 |

In Fig. 3(a)-(e) we display the magnetic contribution to the $Ce_3Sn$ scattering collected from HET at 4.5 and 100 K and at three incident energies (15, 35, and 60 meV). Data from QENS at 7 K (Fig. 3(f)) are included for comparison. The CEF fits are also included (solid lines); as for the $Ce_3In$ case, the fits were performed simultaneously on six different spectra at different incident energies and temperatures. The intensity and form factor of the QENS data have been adjusted to that of the HET spectra at $E_i$=35 meV (spectra (b)) to make a direct comparison. The fitting parameters yield a similar crystal field scheme as for $Ce_3In$: the $\Gamma_7^{(1)}$ doublet is the ground state, $\Gamma_7^{(2)}$ is the first excited state with energy 18.5 meV, and the second excited state is the $\Gamma_6$ doublet at the energy 36.1 meV. The Kondo temperature $T_K = 40$ K is higher than for $Ce_3In$, and the excited state linewidths are broader, reflecting stronger $4f$-conduction hybridization.

Due to the large CEF excitation energies, the low temperature behavior of the magnetic specific heat should be dominated by the $\Gamma_7^{(1)}$ doublet ground state. This is confirmed by the fact that the magnetic entropy (Fig. 4(a) inset) reaches Rln2 near 20 K but only reaches Rln4 near 70 K. For a doublet ground state, the Kondo model predicts $\gamma_0 = \pi R/6T_K$ for the linear coefficient of specific heat[1]. In previous results for $Ce_3In$ a value $T_K = 4.8$ K was deduced using this formula[2]. In addition, the specific heat coefficient $C/T$ showed a peak near 2 K whose existence was somewhat uncertain since the lowest measured temperature was only 1.8 K. We have extended the specific heat measurement down to 400 mK. In Fig. 4(a) we plot $C_{mag}/T$ and find a peak at $T = 2.6$ K. Comparison of the data to the prediction $\gamma^K(T)$ of the Kondo model which is calculated using the value $T_K = \Gamma_{QE}/k_B = 17K$ deduced from our neutron data, shows that the Kondo prediction is much smaller than the experimental value; indeed, $\gamma_0^K$ is only half of $\gamma_{0.4K}^{exp}$ (Table II). Given the large Wilson ratio reported earlier[2], the obvious expla-

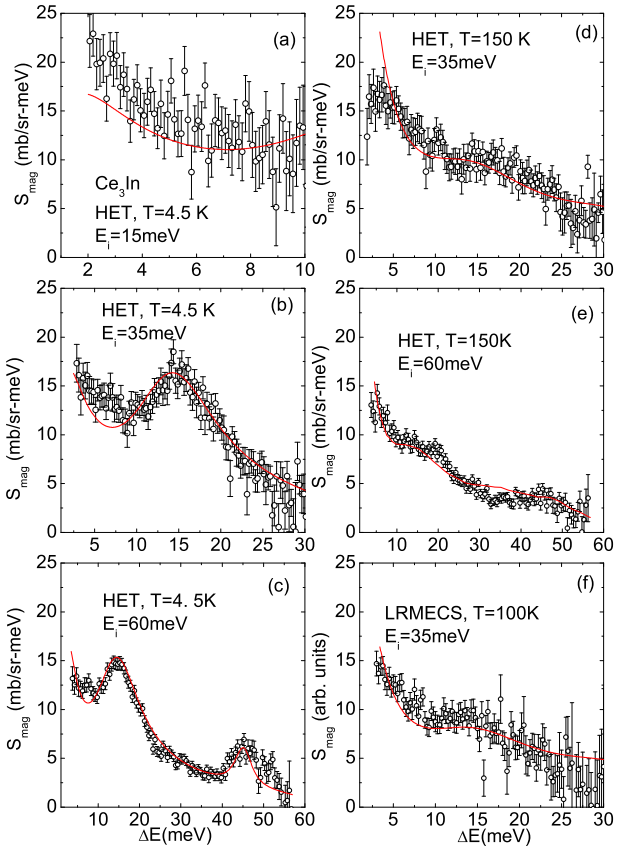


FIG. 2: Magnetic contribution $S_{mag}$ to the inelastic neutron scattering spectra of $Ce_3In$ for data taken on HET at T=4.5 K and 150 K with different incident energies $E_i$=15 meV, 35 meV, and 60 meV and taken on LRMECS at T=100 K with $E_i$=35 meV. The solid lines represent the quasielastic and crystal field contributions obtained from least squares fitting as described in the text.

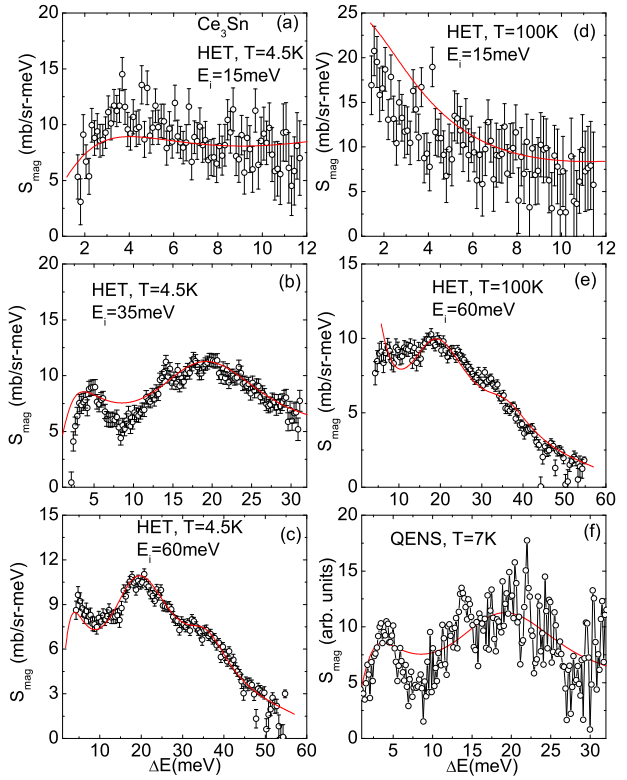


FIG. 3: (a)-(f) Magnetic contribution $S_{mag}$ to the inelastic neutron scattering spectra for $Ce_3Sn$. The temperatures and incident energies are given in the plot. The solid lines represent the CEF model. (f): the magnetic contribution to the INS spectra collected from QENS at 7 K. The solid line in (f) is the CEF model fit for the $E_i$ = 35 meV spectra.

nation is that ferromagnetic (FM) fluctuations dominate the low temperature specific heat, increasing the specific heat above the Kondo value and giving rise to the peak at 2.6 K representing the onset of short range FM order.

We next consider the high temperature susceptibility, comparing the measured value to the value calculated from the crystal field parameters of Table I in the inset of Fig. 4(b). A molecular-field $\lambda$ = 62 mole-Ce/emu has been added to compensate the reduction of the susceptibility at high temperature due to the Kondo effect ($1/\chi^{HT} = 1/\chi^{CEF} + \lambda$). At high temperatures, when the crystal field states are excited, the effective Kondo temperature $T_K^{HT}$ is larger than the Kondo temperature of the ground state doublet. The molecular field constant is related to the effective Kondo temperature via $\lambda = T_K^{HT}/C_{5/2}$ where $C_{5/2}$ is the free ion Curie constant for cerium. This relation gives $T_K^{HT}$ = 77 K, which value is essentially equal to the width $\Gamma_1$ of the first excited level seen in the neutron scattering (Fig. 2 and table I).

At low temperatures, there should be three contributions to $\chi(T)$, as well as to $M(H)$ and $C_{mag}$: one from the Kondo single ion impurity physics of the ground state doublet, one from the FM fluctuations, and one from the excitation of higher lying crystal field states. To carry out such an analysis, we note first that in the $Cu_3Au$ crystal structure, the tetragonal crystal field axis (i.e. the z-axis for the doublet wave functions) points perpendicular to the face containing any given face-centered cerium atom; hence there are three orthogonal tetragonal axes in the unit cell. When applying a magnetic field in a polycrystalline sample, the field will point along the tetragonal axis for $\frac{1}{3}$ of the cerium atoms but orthogonal to the tetragonal axis (in the $x-y$ plane) for $\frac{2}{3}$ of the atoms. The effective low temperature Curie constant is then $C_{eff} = \frac{1}{3}C_{eff}^{z} + \frac{2}{3}C_{eff}^{x}$, where $C_{eff}^{z(x)} = N(g_{eff}^{z(x)}\mu_B)^2\frac{1}{2}(\frac{1}{2}+1)/3k_B$. This is the form for a pseudo spin $\frac{1}{2}$ doublet where the CEF physics is absorbed into the effective $g$-factor. Here $g_{eff}^{z(x)} = \frac{12}{7} < J_{z(x)} >$ where $< J_{z(x)} >$ is the matrix element of the angular moment component along the $z(x)$ axis. From the CEF mixing parameter $\eta$, we determine $C_{eff}$ to be 0.48 emu-K/mole-Ce for $Ce_3In$ and 0.41 emu-K/mole-Ce for $Ce_3Sn$. (Table

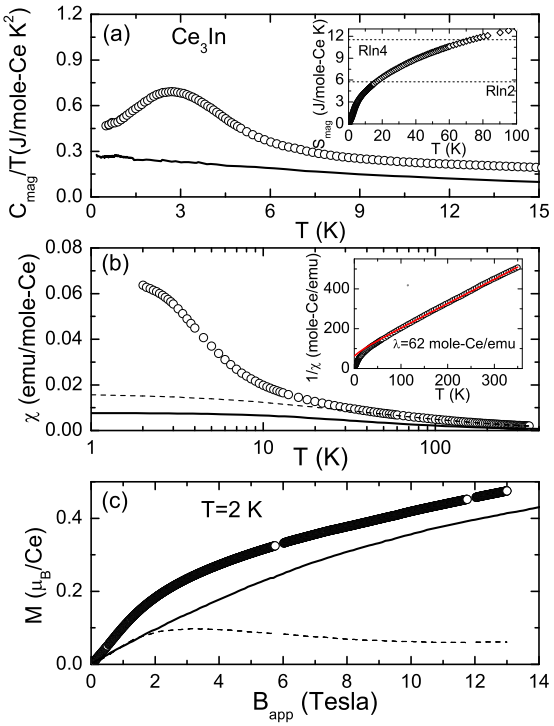


FIG. 4: (a) The magnetic contribution to the specific heat $C_{mag}/T$ versus $T$ for $Ce_3In$. The solid line is the Kondo prediction $\gamma^K(T)$ calculated using $T_K = \Gamma_{QE}/k_B = 17$ K. The inset is the magnetic entropy of $Ce_3In$. (b) The magnetic susceptibility $\chi(T)$ for $Ce_3In$. The solid line is the Kondo prediction $\chi^K(T)$ calculated using $T_K = 17$ K and the low temperature Curie constant determined as described in the text. The dashed line gives the sum of the Kondo and crystal field contributions $\chi^{CEF+K} = \chi^K + (\chi^{CEF} - \chi^{LT}_{Curie})$. The inset is the inverse susceptibility together with the calculated susceptibility (solid line) $1/\chi^{HT} = 1/\chi^{CEF} + \lambda$ obtained using the CEF fitting parameters in table I. (c) The magnetization for $Ce_3In$. The solid line $M^K(B)$ is the Kondo calculation calculation using $T_K = 17$ K. The dashed line is the contribution from the ferromagnetic fluctuations.

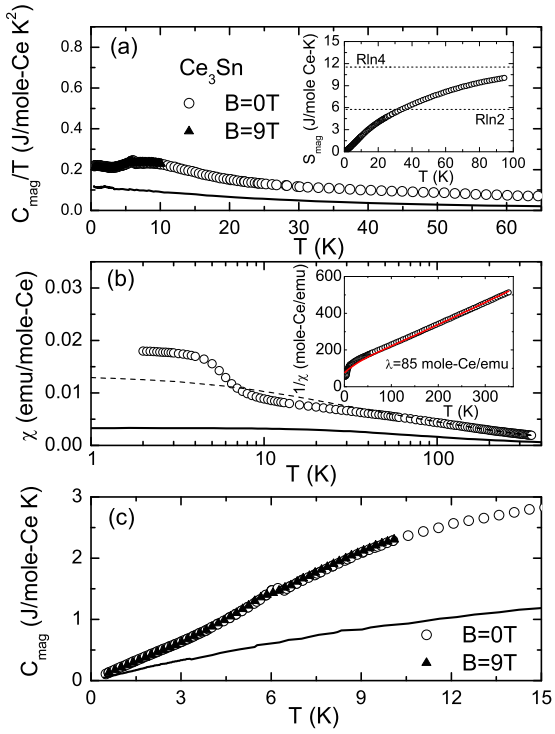


FIG. 5: (a) the magnetic specific heat $C_{mag}/T$ versus $T$ at B=0 T (open circle) and B=9 T (solid triangle) for $Ce_3Sn$. The solid line is the Kondo contribution $\gamma^K(T)$ for $T_K = 40$ K. The inset is the magnetic entropy. (b) Magnetic susceptibility $\chi(T)$ for $Ce_3Sn$. The solid line is the Kondo contribution $\chi^K(T)$ calculated with $T_K = \Gamma_{QE}/k_B = 40$ K and the dashed line is the sum of the Kondo and CEF contributions $\chi^{CEF+K} = \chi^K + (\chi^{CEF} - \chi^{LT}_{Curie})$. The inset is the inverse susceptibility together with the value $1/\chi^{HT} = 1/\chi^{CEF} + \lambda$ (solid line) calculated from CEF fitting parameters in table I. (c) $C_{mag}$ at $B$=0 T (open circle) and B=9 T (solid triangle) for $Ce_3Sn$. The thin solid line is $C^K(T)$ calculated with $T_K =$ 40 K.

II).

To sort the low temperature susceptibility into Kondo, FM, and CEF contributions, we note that since the first CEF excited level is at 152 K, at sufficiently low temperatures the Zeeman splitting of the $\Gamma_7^{(1)}$ ground state doublet will obey a Curie law $\chi^{LT}_{Curie} = C^{LT}_{eff}/T$. Due to the Kondo effect, this Curie behavior will be replaced by the Kondo contribution $\chi^K$, which we calculate using the same Curie constant $C^{LT}_{eff}$ and using $T_K = 17$ K (solid line, Fig. 4(b)). The susceptibility from the combination of the ground state Kondo and the excited crystal fields will then be of the form $\chi^{CEF+K} = \chi^K + (\chi^{CEF} - \chi^{LT}_{Curie})$ where we subtract $\chi^{LT}_{Curie}$ to avoid double counting the ground state contribution. As for the specific heat, the resulting $\chi^{CEF+K}$ (dashed line in Fig. 4(b)) is much smaller than the experimental value at $T < 20$ K. The excess can be viewed as the contribution from the ferromagnetic fluctuations. Taking the latter to be equal to the difference $\chi^{exp} - \chi^{CEF+K}(T)$, the FM contribution is seen to increase below 10 K in a manner characteristic of ferromagnetic short range order.

In Fig. 4(c) we exhibit the magnetization as measured up to 13 Tesla at $T$=2 K. Based on Hewson's calculation of Kondo model[10], we can estimate the Kondo contribution to the magnetization. Since the effective $g$-factors differ in the $z$ and $x-y$ directions, we calculate $M^K = \frac{1}{3}M^K(z) + \frac{2}{3}M^K(xy)$. The result is plotted as a solid line in Fig. 4(c). After subtracting the Kondo contribution, we obtain the contribution from the FM correlations (dashed line). This saturates at a relatively small field $B \sim 2.5$ tesla with $M^{sat} = 0.095\ \mu_B$, which is 10 percent of the saturation value 1.0 $\mu_B$ expected based on the effective $g$-factors.

In the same way as for $Ce_3In$, we calculate $\chi^K(T)$, $\chi^{CEF}(T)$, $\chi^{CEF+K}(T)$, $\gamma^K(T)$ and $C^K(T)$ for $Ce_3Sn$,

TABLE II: Kondo single ion model calculation for $Ce_3In$ and $Ce_3Sn$.

| | $< J_z >$ | $< J_x >$ | $M^{sat}_{CEF}$ | $C^{LT}_{eff}$ | $\chi^K_0(\frac{emu}{mole-Ce})$ | $\gamma^K_0(\frac{J}{moleCeK^2})$ | $\chi^{exp}_{0.4K}(\frac{emu}{mole-Ce})$ | $\gamma^{exp}_{0.4K}(\frac{J}{moleCeK^2})$ |
|---|---|---|---|---|---|---|---|---|
| $Ce_3In$ | 2.0344 | 0.7171 | 0.991 | 0.4765 | 0.0076 | 0.256 | 0.064 | 0.467 |
| $Ce_3Sn$ | 1.6684 | 0.9074 | 0.994 | 0.4086 | 0.0033 | 0.109 | 0.018 | 0.221 |

comparing to the measured data in Fig. 5. The high temperature susceptibility (Fig. 5(b) inset) can again be fit with the sum of the CEF contribution calculated using the parameters of Table I and a molecular field contribution (solid line). The value $\lambda = 85$ mole-Ce/emu of molecular field constant implies an effective Kondo temperature at high temperature $T_K^{HT} = 105$ K, which again is essentially equal to the linewidth 9.4 meV of the first excited state seen in the neutron scattering (Table I).

The solid lines in Fig. 5 represent the Kondo ground state doublet contributions. In Fig. 5(b), the dashed line is $\chi^{CEF+K}(T)$. The excess due to the FM correlations has a much smaller magnitude ($\sim$ 0.005 emu/mol-Ce) than for $Ce_3In$ where the FM contribution is of order 0.05 emu/mol-Ce. A similar statement holds for the FM contribution to the specific heat coefficient, which is of order 0.4 J/mol-Ce-$K^2$ for $Ce_3In$ but only 0.1 J/mol-Ce-$K^2$ for $Ce_3Sn$ (Figs. 4(a) and 5(b)). Hence the FM enhancement is smaller in $Ce_3Sn$ than in $Ce_3In$, consistent with the larger value of $T_K$.

In order to better understand these compounds, we measured the specific heat of $Ce_3In$ under different applied fields (B = 0 T, 1 T, 3 T, 6 T and 9 T). The results for the magnetic contribution $C_{mag}$ are shown in Fig. 6. The low temperature peak in $C_{mag}$ moves to higher temperature when the field is increased. Since the peak in the Kondo contribution to $C_{mag}$ is expected to increase with field, we plot in Fig. 6(a)-(e) the Kondo contribution $C^K(B)$ calculated for different applied fields using the theoretical results of Sacramento and Schlottmann[11]. In calculating $C^K(B)$, we again account for the different effective $g$-factors in the $z$ and $x-y$ directions. The results indicate that the Kondo contribution is not expected to alter significantly in applied fields of order 9 T, essentially because $g_{eff}\mu_B B < k_B T_K$ for these fields. This makes it clear that the peak does not arise from the Kondo scattering but must be due to the FM fluctuations.

To quantify the FM contribution, we again assume that the measured magnetic specific heat is the sum of the ground state doublet Kondo contribution $C^K(B)$, the FM contribution $C^{FM}$, and a contribution $C^{CEF}$ due to the excitation of higher lying CEF states. Since the FM fluctuations appear to only contribute to the susceptibility below 10 K (Fig. 4 b) we assume that the excess $C_{mag}$ - $C^K(B)$ observed for $T > 10$ K is primarily due to CEF excitations. Given the large linewidths of the CEF excitations seen in the neutron scattering, and concomitant large effective $T_K^{HT}$ at high temperature, this contribution to the specific heat is much broader as a function of temperature than would be the case for a simple CEF Schottky anomaly. For simplicity, we approximate this CEF contribution as linear in temperature, with slope equal to that observed in the range 8-15 K, and we assume that since the CEF excitation energy is large, this contribution will be unaffected by fields of order 9 T. We approximate the FM contribution $C^{FM}$ as a Gaussian, centered at a temperature that increases with field. The three contributions, Kondo, CEF, and FM, are plotted at the different fields in Figs. 6(a)-(e). The solid lines, which represent the sum of all three contributions, fit the data very well at all fields.

We plot the Gaussian peak temperature in Fig. 6(f), where it is seen to grow linearly with field. This suggests Zeeman splitting, where at zero field the splitting arises from the internal field in the regions of FM short range order, and where the applied field increases the splitting. To determine the internal field $B_{int}$, we calculate the Schottky anomaly $C^{Schotkky}(B_{int})$ expected due to Zeeman splitting of a doublet with the same effective $g$-factors as we have obtained from the neutron fits; we then adjust $B_{int}$ until the peak temperature of the Schottky anomaly is the same as that of the Gaussian peak temperature for $B = 0$. This gives $B_{int} = 9.5$ T. We then calculate $C^{Schottky}(B_{int} + B_{app})$ to determine peak position of the Schottky anomaly in an applied field $B_{app}$. As can be seen in Fig. 6 (f), the Gaussian peak temperatures track the expected Zeeman splitting very closely. On the other hand, the temperature dependence of the Schottky specific heat calculated in this manner is considerably broader than the Gaussian contributions $C^{FM}$ that are plotted in Fig. 5. This means that, while the contribution of the FM short range order to the specific heat is not of Schottky form, the increase of the Gaussian peak position is the same as the Zeeman splitting expected for a total field $B_{int} + B_{app}$ given the effective $g$-factors.

The entropy of the Gaussian contribution is about 15 % of Rln2 for all fields. This corresponds to the estimate obtained from the magnetization $M(B)$ where the saturation value of the FM contribution is about 10% of the value 1.0 $\mu_B$ expected for the $\Gamma_7^{(1)}$ ground state doublet for the measured value of $\eta$. Hence, the enhancement of $\chi_0$ and $\gamma_0$ arises from magnetic fluctuations which involve 10-15 % of the $4f$ electron degrees of freedom.

In Fig. 5(c), we compare the magnetic specific heat $C_{mag}$ at zero field and $B = 9$ T for $Ce_3Sn$. The solid line is the Kondo contribution $C^K$. The specific heat does not change with field for $B < 9$ T. The most likely explanation of this is that, as discussed above, the FM

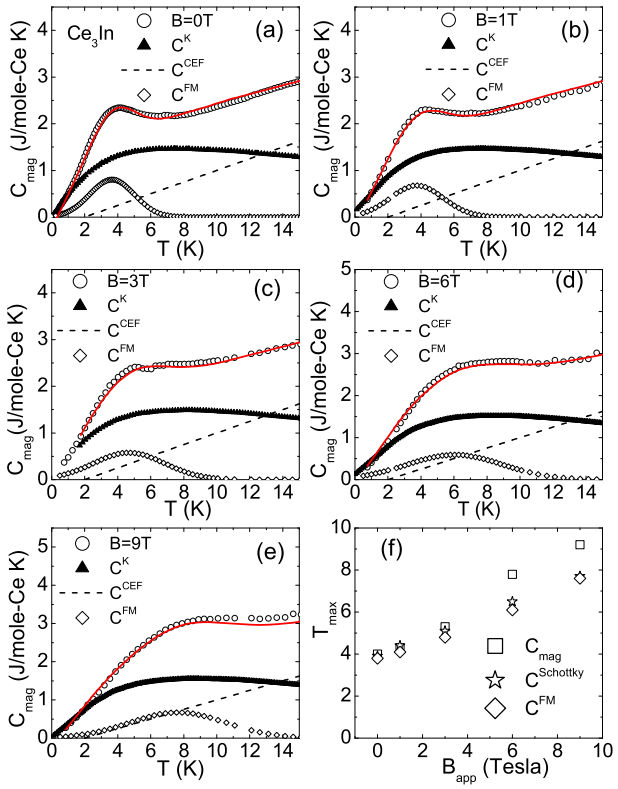


FIG. 6: (a), (b), (c), (d) and (e): $C_{mag}$ of $Ce_3In$ in different applied magnetic fields. The solid line sums the three contributions (Kondo, CEF, and FM fluctuations) shown in the plot. (f): The peak position of $C_{mag}$, of the Gaussian contribution $C^{FM}$ due to the FM fluctuations, and the expected peak position in the Schottky anomaly $C^{Schottky}(B_{int}+B_{app})$ due to Zeeman splitting in the presence of an internal field $B_{int}$.

correlations make a smaller contribution than in $Ce_3In$. The excess specific heat $C_{mag} - C^K$ seen for $T > 6$ K is presumably due to the CEF contribution, which should be even broader in temperature in $Ce_3Sn$ than in $Ce_3In$ due to the larger Kondo temperature.

We have demonstrated that the large $\gamma$ observed in $Ce_3In$ arises more from ferromagnetic correlations than from the single ion Kondo physics. This reflects the fact that the system is close to a ferromagnetic quantum critical point. In a $Q$-resolved INS experiment, the ferromagnetic correlations should show up in the vicinity of $Q$ =0 riding on a background of $Q$ independent Kondo scattering. We can estimate that these FM correlations will have 10-15% of the total spectral weight in $Q$-space. Since the large $\gamma$ and the proximity to the QCP occurs when the Kondo temperature $T_K$ = 17 K is fairly large, it is also reasonable to believe that when an appropriate control parameter (e.g. alloying parameter x in $Ce_{3-x}La_xIn$) drives this system to the QCP, the Kondo temperature $T_K$ will remain finite, as expected for example for a spin density wave type QCP.

We have observed strong FM fluctuations in the related compound $Pr_3In$, which is an antiferromagnet below 12 K[16]. A possibility for this behavior is that AFM interactions between rare earth atoms on the face centers of the $Cu_3Au$ structure are frustrated. If, for example, the atoms at (1/2 1/2 0) and (1/2 0 1/2) are aligned antiferromagnetically, the atom at (0 1/2 1/2) will be free to point to any direction. Ferromagnetic next-nearest-neighbor interactions could then stabilize ferromagnetism on this sublattice[17]. In any case, the FM correlations appear to be generic to this crystal structure.

In conclusion, we have used inelastic neutron scattering to determine the crystalline electric field (CEF) splitting and Kondo energy scale in $Ce_3In$ and $Ce_3Sn$. For both compounds the crystal field excitation energy is large. For $Ce_3In$ we have separated the magnetization $M(B)$, susceptibility $\chi(T)$ and specific heat $C_{mag}$ into contributions from the Kondo effect, from the CEF, and from FM fluctuations. The simplified model calculation for $Ce_3In$ shows that the FM correlations make a 15 % contribution to the doublet ground state entropy and that the large $\gamma$ arises mostly from the FM correlations. This suggests $Ce_3In$ is close to a quantum critical point (QCP). The Kondo temperature $T_K$ is expected to remain finite at the QCP, as occurs for a spin density wave type QCP. INS experiments in single crystals of these compounds would be very interesting.

## IV. ACKNOWLEDGEMENTS

We thank Vivien Zapf for her assistance in the measurement at NHMFL and Cristian Batista for his insightful comments. Research at UC Irvine was supported by the U.S. Department of Energy, Office of Basic Energy Sciences, Division of Materials Sciences and Engineering under Award DE-FG02-03ER46036. Work at ORNL was supported by the Scientific User Facilities Division Office of Basic Energy Sciences, DOE and was managed by UT-Battelle, LLC, for DOE under Contract DE-AC05-00OR22725. Work at Los Alamos National Laboratory was performed under the auspices of the U.S. DOE/Office of Science. Work at NHMFL-PFF, Los Alamos was performed under the auspices of the National Science Foundation, the State of Florida, and U.S. DOE. Work at ANL was supported by DOE-BES under contract DE-AC02-06CH11357.

[1] V. T. Rajan, Phys. Rev. Lett., 51, 308 (1983).

[2] Y. Y. Chen, J. M. Lawrence, J. D. Thompson and J. O.

Willis, Phys. Rev. B **40**, 10766(1989).
[3] J. M. Lawrence, Y. Y. Chen, J. D. Thompson and J. O. Willis, Physica B **163**, 56-58(1990).
[4] H. Kadowaki, M. Sato and S. Kawarazaki, Phys. Rev. Lett. **92**, 097204 (2004).
[5] H. Kadowaki, B. Fk, T. Fukuhara, K. Maezawa, K. Nakajima, M. A. Adams, S. Raymond and J. Flouquet, Phys. Rev. B **68**, 140402 (2003).
[6] J. M. Lawrence, S. M. Shapiro, J. L. Sarrao and Z. Fisk, Phys. Rev. B **55**, 14467 (1997).
[7] J. M. Lawrence, P. S. Riseborough, C. H. Booth, J. L. Sarrao, J. D. Thompson, and R. Osborn, Phys. Rev. B **63**, 054427 (2001).
[8] I. Aviani, M. Miljak and V. Zlatic, Phys. Rev. B **64**, 184434 (2001).
[9] G. Fischer and A. Herr, Phys. Stat. Sol. B **141**, 589 (1987).
[10] A. C. Hewson, J. W. Rasul, J. Phys. C: Solid State Phys. **16**, 6799 (1983).
[11] P. D. Sacramento and P. Schlottmann, Phys. Rev. B **40**, 431 (1989).
[12] A. P. Murani, Phys. Rev. B **28**, 2308 (1983).
[13] E. A. Goremychkin, R. Osborn, Phys. Rev. B **47**, 14280 (1993).
[14] J. M. Lawrence, P. S. Riseborough, C. H. Booth, J. L. Sarrao, J. D. Thompson and R. Osborn, Phys. Rev. B **63**, 054427 (2001).
[15] Experimental probes of CEF excitations can not distinguish between a positive and a negative value of $B_4^4$. Only the modulus is observable. Consequently the distinction between the $\Gamma_7^{(1)}$ and $\Gamma_7^{(2)}$ states is a matter of convention ( A. D. Christianson et al. Phys. Rev. B **70**, 134505 (2004)).
[16] A. D. Christianson, J. M. Lawrence, J. L. Zarestky, H. S. Suzuki, J. D. Thompson, M. F. Hundley, J. L. Sarrao, C. H. Booth, D. Antonio, A. L. Cornelius, Phys. Rev. B 72, 024402 (2005).
[17] Cristian Batista, private communication.